第 34 卷 第 3 期 原 子 核 物 理 评 论 Vol. 34, No. 3
2017 年 9 月 Nuclear Physics Review Sep., 2017

Article ID: 1007-4627(2017) 03-0338-06

Investigations of Cluster Effects in Atomic Nuclei

REN Zhongzhou[1,2], LÜ Mengjiao[1], WAN Niu[1]

(*1. Department of Physics, Nanjing University, Nanjing 210093, China;*
2. Center of Theoretical Nuclear Physics, National Laboratory of Heavy-Ion Accelerator, Lanzhou 730000, China)

Abstract: We introduce our recent works on the clustering effects in atomic nuclear systems. The clustering structures for ^{20}Ne and ^{9,10}Be isotopes are studied with the Tohsaki-Horiuchi-Schuck-Röpke (THSR) wave function. It is found that a single THSR wave function can provide good description for the cluster state. The nonlocalised aspect of cluster dynamics is discovered with the hybrid-THSR-Brink wave function. Extensions are made for the THSR wave function to enable studies of $N \neq Z$ nuclei. The nuclear molecular orbit structures in low lying states of ^{9,10}Be isotopes are correctly reproduced with this wave function. We also discuss the α-decay processes for proton/neutron-rich nuclei. The effect of proton/neutron skin is found to be considerable on α-decay half-life.

Key words: cluster structure; nonlocalised cluster dynamics; neutron-rich nuclei; α-decay

CLC number: O571.6; P142.9 **Document code:** A **DOI:** 10.11804/NuclPhysRev.34.03.338

1 Introduction

Since the beginning of this century, the clustering degree of freedom has aroused a lot of interest in various branches of nuclear physics[1–17]. This include the discovery of Tohsaki-Horiuchi-Schuck-Röpke (THSR) wave function which has triggered a series of investigations on the nonlocalised dynamics in light nuclei[1–9]. Beside the studies of cluster structures, important progresses have also been achieved for the investigations of α-decay processes[12–15, 17].

In 2001, four authors proposed the THSR wave function based on the α-cluster condensation for the gas-like states of ^{12}C and ^{16}O nuclei[1]. It is then extended to various other clustering systems including $^{8-11}$Be, ^{20}Ne and one-dimension α-cluster systems[2–6]. It is found that the squared overlap between RGM/GCM (Resonating Group Method/Generator Coordinate Method) wave function and a single THSR wave function is almost 100% for both gas-like and non-gas-like states of ^{8}Be, ^{12}C and ^{20}Ne, which proves that the THSR wave function provides good description for these states[2–5]. Also, the nonlocalised dynamics of α-clusters is discovered by the investigation of the inversion-doublet-bands of ^{20}Ne[4].

Along with the continuously successful application on the n-α aggregates, the THSR wave function is further extended to $N \neq Z$ nuclei including various isotopes of Be and B nuclei[7, 8]. In these investigations, the nonlocalised approach is found to prevail for nuclear systems composed of both α-clusters and valence neutrons. Also, the nuclear molecular orbit structure is found to be naturally reproduced by the THSR wave function. These extension enables possibility to study the coupling of clustering degree of freedom and the nucleon degree of freedom, especially for neutron-rich nuclei far away from the β-stability line.

The effects of neutron and proton skin in neutron or proton-rich nuclei on the α decay process is also studied recently[13, 14]. It is found that the introduction of this isospin effect can obviously reduce the deviation between theory and experiments of α-decay half lives. Thus the consideration of isospin effect is found to be necessary for further studies of α-decay half lives.

In this work, we will introduce our recent investigations on the clustering effects for both α-clustering structures and α-decay process. In Sec. 2 we show our studies on ^{20}Ne with the THSR wave function and the nonlocalised dynamics of clusters. Then in Sec. 3 the extension of THSR wave function into $N \neq Z$ and corresponding applications on ^{9,10}Be are introduced. We

Received date: 14 Dec. 2016; **Revised date:** 2 May 2017

Foundation item: National Natural Science Foundation of China (11535004, 11035001, 11375086, 11105079, 10735010, 10975072, 11175085, 11235001); National Basic Research Program of China (973 Program) (2013CB834400, 2010CB327803)

Biography: REN Zhongzhou (1962–), Nanyang, Henan, Professor, working on nuclear physics; E-mail: zren@nju.edu.cn.

will also discuss our recent studies of α-decay process for neutron-rich and proton-rich nuclei in Sec. 4. The last section Sec. 5 contains the conclusion.

2 Cluster structure in ^{20}Ne

The THSR wave function of ^{20}Ne is formulated as Gaussian integration of corresponding Brink wave functions, as

$$\Psi^{\mathrm{THSR}}(\beta_{xy},\beta_z)=\int \mathrm{d}\boldsymbol{R}_1\cdots\mathrm{d}\boldsymbol{R}_n\times \exp\left\{-\frac{R_{i,x}^2+R_{i,y}^2}{\beta_{xy}^2}-\frac{R_{i,z}^2}{\beta_z^2}\right\}\times \Psi^{\mathrm{Brink}}(\boldsymbol{R}_1,\cdots,\boldsymbol{R}_n)\ . \tag{1}$$

Here $\boldsymbol{R}$ is the generator coordinate which denotes the distance between the ^{16}O cluster and the α-cluster inside the ^{20}Ne nucleus. The β parameters constrains these two clusters in a Gaussian style container, which is obtained by variational optimization process. Naturally, this wave function can provide description for states with positive parity[3].

For the negative parity states, another generator coordinate $\boldsymbol{S}$ is introduced, and the hybrid-THSR-Brink wave function is formulated as

$$\Psi^{\mathrm{THSR}}(\beta_{xy},\beta_z)=\int \mathrm{d}\boldsymbol{R}_1\cdots\mathrm{d}\boldsymbol{R}_n\times \exp\left\{-\frac{R_{i,x}^2+R_{i,y}^2}{\beta_{xy}^2}-\frac{R_{i,z}^2}{\beta_z^2}\right\}\times \Psi^{\mathrm{Brink}}(\boldsymbol{R}_1+\boldsymbol{S}_1,\cdots,\boldsymbol{R}_n+\boldsymbol{S}_n)\ . \tag{2}$$

With this new generator coordinate $\boldsymbol{R}+\boldsymbol{S}$ denote the center for each cluster in the Brink wave function. The positive parity in previous THSR wave function is broken, and thus the negative parity state can be extracted by parity projection[4].

In Table 1, the energy spectrum for rotational bands with both positive and negative parity obtained with the THSR wave function are listed and compared with the RGM/GCM results. The squared overlap $|\langle\Psi^{\mathrm{THSR}}|\Psi^{\mathrm{GCM}}\rangle|^2$ is also given in the table. These squared overlaps which almost equal 100% show clearly that one single THSR wave function almost equals the RGM/GCM wave function. In principle, the RGM/GCM wave function is considered the exact solution for the cluster system, thus the THSR wave function is proved to provide correct description for these states.

One of the astonishing aspect of the THSR wave function is that it triggers the concept of nonlocalised cluster dynamics[4]. This can be obtained by the comparison between energy curves with different parameters in the hybrid-THSR-Brink wave function, as shown in Fig. 1. In this figure, the minimum point for each curve with parameter $\beta=0$ locates at finite S_z, which correspond to standard Brink wave functions with two-cluster distance S_z. When parameter β is adopted as the variational optimized value, the minimum points shift to $S_z=0$, which correspond to standard THSR wave functions. It was found that the energy minimum with the THSR wave function is lower than the Brink one, thus the dynamics described by the THSR wave function is more favored than the Brink description. Because of the Gaussian integration of the generator coordinates $\boldsymbol{R}_i$ of two clusters in the THSR wave function, each cluster is thus found to perform a nonlocalised motion in the container constrained by the Gaussian parameters. This nonlocalised aspect is also discussed in other nuclear systems such as the ^{10}Be nucleus[8].

Table 1　Calculated results of the rotational band of ^{20}Ne with both positive and negative parity, taken from Refs. [3, 4]. "E (THSR)" denotes results calculated with the THSR wave function. "E (GCM)" denotes results calculated with the RGM/GCM wave function. "E (Exp)" denotes experimental values. $|\langle\Psi^{\mathrm{THSR}}|\Psi^{\mathrm{GCM}}\rangle|^2$ is the squared overlap between the THSR wave function and the RGM/GCM wave function. All units are in MeV.

	E (THSR)	E (GCM)	E (Exp)	$\lvert\langle\Psi^{\mathrm{THSR}}\rvert\Psi^{\mathrm{GCM}}\rangle\rvert^2$
0^+	−159.85	−160.05	−160.64	0.992 9
2^+	−158.53	−158.84	−159.01	0.987 9
4^+	−155.50	−156.04	−156.39	0.977 5
1^-	−155.38	−155.38	−154.85	0.999 8
3^-	−153.07	−153.08	−153.49	0.998 7

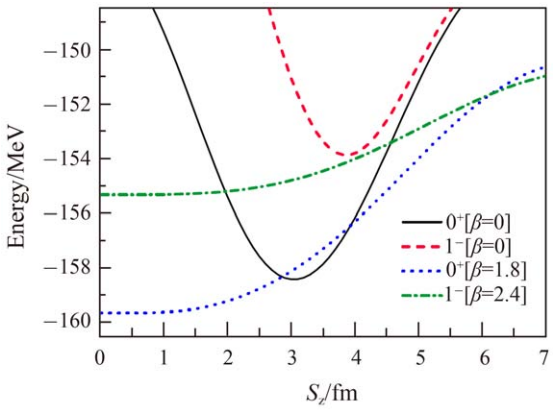

Fig. 1　(color online) Energy curves of $J^\pi=0^+,1^-$ states with different parameters in the hybrid-THSR-Brink wave function, taken from Ref. [4].

3 Cluster structure in ^{9,10}Be isotopes

The THSR wave function is further extended to the $N \neq Z$ isotopes ^{9,10}Be which consist of both α-clusters and valence neutrons. The formulation of the extended THSR wave function can be described as

$$\left|\Phi(^{9-10}\mathrm{Be})\right\rangle = (C_\alpha^\dagger)^2 (c_\mathrm{n}^\dagger)^{1-2} |\mathrm{vac}\rangle \ , \tag{3}$$

where the $C_\alpha^\dagger$ is the creation operators of α-clusters as used in previous section and $c_\mathrm{n}^\dagger$ is the creation operators of valence neutrons. The form of $c_\mathrm{n}^\dagger$ depends on the parity of the single neutron wave function. For the ground state of ^{9}Be and ^{10}Be, valence neutrons are supposed to occupy π-orbit states with negative parity, with corresponding $c_\mathrm{n}^\dagger$ as

$$c_{\mathrm{n},\sigma}^\dagger = \int \mathrm{d}^3\boldsymbol{R}_\mathrm{n} \exp\left(-\frac{R_{\mathrm{n},x}^2}{\beta_{\mathrm{n},xy}^2} - \frac{R_{\mathrm{n},y}^2}{\beta_{\mathrm{n},xy}^2} - \frac{R_{\mathrm{n},z}^2}{\beta_{\mathrm{n},z}^2}\right) \mathrm{e}^{\mathrm{i}m\phi_{\boldsymbol{R}_\mathrm{n}}} \times \int \mathrm{d}^3\boldsymbol{r}_\mathrm{n} \times (\pi b^2)^{-3/4} \mathrm{e}^{-\frac{(\boldsymbol{r}_\mathrm{n}-\boldsymbol{R}_\mathrm{n})^2}{2b^2}} a_{\sigma,\mathrm{n}}^\dagger(\boldsymbol{r}_\mathrm{n}) \ . \tag{4}$$

As discussed in Ref. [7], this creation operator with extra phase factor $\mathrm{e}^{\mathrm{i}m\phi_{\boldsymbol{R}_\mathrm{n}}}$ ensures the negative parity in this THSR wave function. For the second 0^+ state of ^{10}Be, the valence neutron is supposed to occupy the linear-chain-like σ-orbit with positive parity. This can be described by the creation operator $c_\mathrm{n}^\dagger$ as

$$c_{\mathrm{n},\sigma}^\dagger = \int \mathrm{d}R_{\mathrm{n},z}(D - |R_{\mathrm{n},z}|) \exp\left(-\frac{R_{\mathrm{n},z}^2}{\beta_{\mathrm{n},z}^2}\right) \int \mathrm{d}^3\boldsymbol{r}_\mathrm{n} \times (\pi b^2)^{-3/4} \mathrm{e}^{-\frac{(\boldsymbol{r}_\mathrm{n}-\boldsymbol{R}_\mathrm{n})^2}{2b^2}} a_{\sigma,\mathrm{n}}^\dagger(\boldsymbol{r}_\mathrm{n}) \ , \tag{5}$$

where parameter D determines the node structure.

In Table 2 we show the energy spectrum for some low lying states of ^{9,10}Be calculated with the THSR wave function. It is clearly shown that the calculated energies with a single THSR wave function agree well with RGM/GCM or Antisymmetrized Molecular Dynamics (AMD) results. From the squared overlap $|\langle\Psi^{\mathrm{THSR}}|\Psi^{\mathrm{GCM}}\rangle|^2$ for the low lying states of ^{9}Be which is about 95%, we found that the extended THSR wave function is very suitable for the description of these states. This conclusion is similar to our previous discussions for the ^{20}Ne nucleus, which shows that the THSR anstaz prevails when extra valence neutrons are introduced.

Also, in Fig. 2 and Fig. 3, we show two rotational bands of ^{10}Be comparing with the AMD results and experimental data. In these figures, results calculated with THSR wave function and di-neutron correlation are also included. It is found that the rotational bands obtained with single THSR wave function agree with the AMD results. Also, small improvement can be observed after the introduction of di-neutron correlation in the THSR wave function.

Table 2 Calculated results of some low lying states of ^{9,10}Be isotopes. "E (THSR)" denotes results calculated with the THSR wave function. "E (GCM)" denotes results calculated with the RGM/GCM wave function. "E (AMD)" denotes results calculated with the AMD method. "E (Exp)" denotes experimental values. All units are in MeV.

	E(THSR)	E(GCM)	E(AMD)[18, 19]	E(Exp)
^{9}Be($3/2^-$)	−55.4	−56.4	–	−58.2
^{9}Be($5/2^-$)	−53.0	−53.8	–	−55.8
^{9}Be($7/2^-$)	−48.6	−49.4	–	−51.8
^{10}Be(0_1^+)	−58.2	–	−60.4	−65.0
^{10}Be(0_2^+)	−50.0	–	−52.3	−58.8

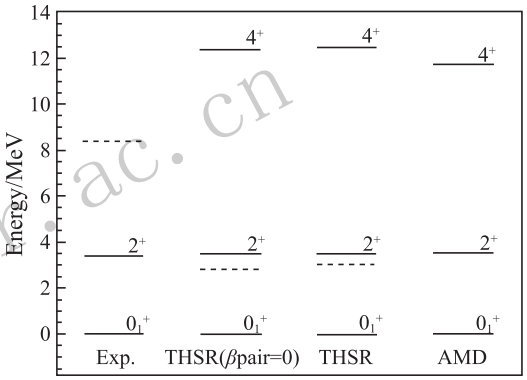

Fig. 2 The 0^+ ground state of ^{10}Be and its rotational band, taken from Ref. [8]. "THSR,ind" and "THSR,cor" denote calculated results with the independent THSR wave function and the correlated THSR wave function, respectively. "AMD" denotes the calculated results of the AMD method[19]. "Exp." denotes the experimental result. The dashed lines indicate the corresponding $\alpha+\alpha+$ n + n threshold −55.2 MeV.

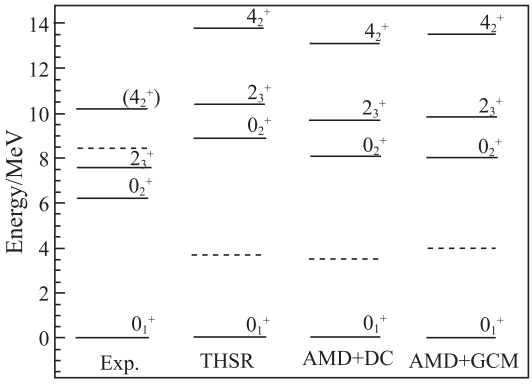

Fig. 3 Energy spectrum of the 0_2^+ rotational band relative to the ground state energy, taken from Ref. [8]. The one labeled with "AMD+DC" is the value calculated with the AMD+DC method[19]. The one labeled with "AMD+GCM" is the value calculated with the $\beta-\gamma$ constrained AMD+GCM method[20]. The dashed lines are the corresponding $\alpha+\alpha+$n + n thresholds of −55.2 MeV.

The structure of these cluster states is discussed by showing the density distribution of valence neutrons as in Fig. 4 and Fig. 5. Here we find that the density distribution of the valence neutron shows a standard π-orbit structure for the ground state of ^{10}Be. And for the second 0^+ state of ^{10}Be, the density distribution has an obvious linear-chain-like σ-orbit structure. Usually, these nuclear molecular orbits are described by superposition of many bases in theoretical models. Thus, it is interesting to obtain the single THSR wave function which already provides good description for nuclear molecular structure.

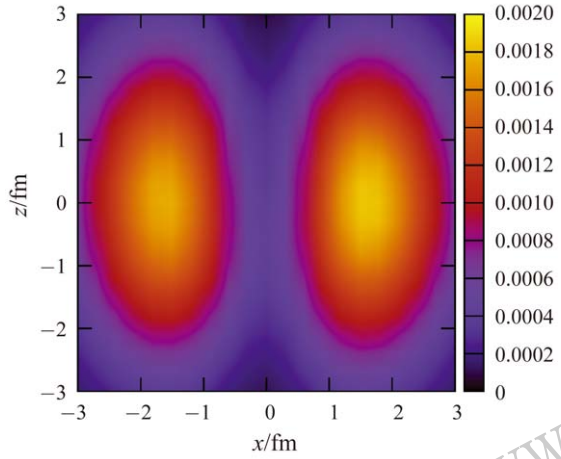

Fig. 4 (color online) Density distribution of valence neutrons in the intrinsic 0_1^+ state of ^{10}Be, taken from Ref. [8]. The color scale of each point in the figure is proportional to the nucleon density in the $x-z$ plane of the $y=0$ cross section. The unit of the density is fm^{-3}.

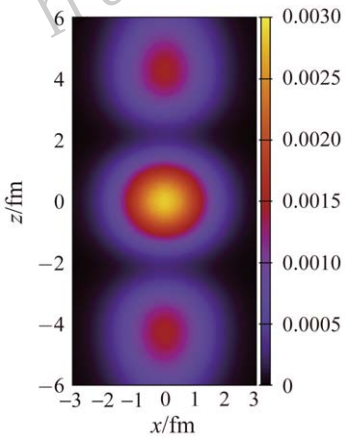

Fig. 5 (color online) Density distribution of valence neutrons in the intrinsic 0_2^+ state of ^{10}Be, taken from Ref. [8]. The color scale of each point in the figure is proportional to the nucleon density in the $x-z$ plane of the $y=0$ cross section. The unit of the density is fm^{-3}.

One of the important characteristics of the extended THSR wave function is that it enables studies of neutron-rich nuclei with the nonlocalised clustering approach. In our future publications, we will introduce further investigations of more neutron-rich isotopes of Be element.

4 α-decay process in neutron/proton rich nuclei

We also investigate the α-cluster decay process in neutron-rich or proton-rich nuclei[13, 14]. Here a simplified α-decay model[21, 22] is adopted to study the effects of neutron and proton skins in neutron or proton-rich nuclei on the α-decay process. In this model, only the point-charge Coulomb potential $V_{\rm C}(R)=Z_1Z_2e^2/R$ operates beyond mother nucleus surface, where Z_1 and Z_2 are the proton numbers of the α particle and daughter nucleus, respectively. Then the α-decay half-life can be analytically derived as

$$T_{1/2}=\frac{\hbar\ln 2}{P_\alpha F\frac{\hbar^2}{4\mu}\exp\left[-2\int_{R_2}^{R_3}\sqrt{\frac{2\mu}{\hbar^2}|Q-V_{\rm C}(R)|}{\rm d}R\right]}, \tag{6}$$

where P_α is the α preformation probability and F is a normalization factor defined by the two-potential approach[23]. μ is the reduced mass of α-core system and Q is the α-decay energy. R_2 and R_3 are the second and third classical turning points, respectively. The centrifugal potential is not involved since only favored α decays are investigated here. By inserting the two relations $R_2=R_d+R_\alpha$ and $R_3=Z_1Z_2e^2/Q$ into Eq. (6), one can obtain[12, 17, 21, 22]

$$\log_{10}T_{1/2}=a\sqrt{\mu}Z_1Z_2Q^{-1/2}+b\sqrt{\mu Z_1Z_2(R_{\rm d}+R_\alpha)}+c, \tag{7}$$

where R_α and $R_{\rm d}$ are the the radii of α-particle and daughter nucleus, respectively. Here the parameters $a=\frac{\sqrt{2}\pi e^2}{\hbar\ln 10}$, $b=-\frac{4e\sqrt{2}}{\hbar\ln 10}$ and $c=\log_{10}\frac{4\mu\ln 2}{\hbar P_\alpha F}$ are obtained by fitting experimental data since the point-charge Coulomb potential is assumed and P_α and F are not always constants. The radius $R_{\rm d}$ is obtained from the simple relation with the root-mean square (rms) radius: $R_{\rm rms}=\sqrt{\frac{3}{5}}R_{\rm d}$[24]. The latter can be calculated from the proton and neutron density distributions $\rho_{\rm p/n}(r)=\rho^0_{\rm p/n}/\{1+\exp[(r-c_{\rm p/n})/a_{\rm p/n}]\}$ of daughter nucleus $R_{\rm rms}=\sqrt{\int 4\pi[\rho_{\rm p}(r)+\rho_{\rm n}(r)]r^4{\rm d}r/A_2}$, where A_2 is the mass number of the daughter nucleus. Here we use the so-called proton and neutron skins to characterize the difference between $\rho_{\rm p}(r)$ and $\rho_{\rm n}(r)$

$$S_{\rm p}=R_{\rm p}-R_{\rm n},\qquad S_{\rm n}=R_{\rm n}-R_{\rm p}\ , \tag{8}$$

where $R_{\rm p}=\sqrt{\int 4\pi\rho_{\rm p}(r)r^4{\rm d}r/Z_2}$ is the proton rms radius and $R_{\rm n}=\sqrt{\int 4\pi\rho_{\rm n}(r)r^4{\rm d}r/N_2}$ is the neutron one. $N_2=A_2-Z_2$ is the neutron number of the daughter nucleus.

Since the proton and neutron density distributions and the neutron skin of the double-magic nucleus ^{208}Pb was extracted with the parameters $a_{\rm p}=0.447$ fm, $c_{\rm p}=6.680$ fm, $a_{\rm n}=0.55$ fm and $c_{\rm n}=6.70$ fm[25], here we only explore the effect of the skin S on the α-decay half-life $T_{1/2}$ for α emitters decaying to ^{208}Pb, isotopes of $Z_2=82$ and isotopes of $N_2=126$. The half-density radii $c_{\rm p/n}$ and diffuseness parameters $a_{\rm p/n}$ of the density distributions $\rho_{\rm p/n}(r)=\rho^0_{\rm p/n}/\{1+\exp[(r-c_{\rm p/n})/a_{\rm p/n}]\}$ for these daughter nuclei are given as follows:

$$\begin{cases}\text{For isotopes of } Z_2=82:\\ \quad a_{\rm p}=0.447 \text{ fm and } c_{\rm p}=6.680 \text{ fm};\\ \quad a_{\rm n}=0.55 \text{ fm and } c_{\rm n}=1.1308A_2^{1/3} \text{ fm};\\ \text{For isotopes of } N_2=126:\\ \quad a_{\rm p}=0.447 \text{ fm and } c_{\rm p}=1.1274A_2^{1/3} \text{ fm};\\ \quad a_{\rm n}=0.55 \text{ fm and } c_{\rm n}=6.70 \text{ fm},\end{cases} \tag{9}$$

where the values 1.1308 and 1.1274 are obtained by fitting the experimental values of ^{208}Pb[25].

By using Eq. (8) and Eq. (9), the skins in these daughter nuclei are calculated, as shown in Fig. 6. It is clearly seen from Fig. 6 that the skin thickness varies smoothly with the neutron number either for the proton skin case or the neutron skin case for both isotopes of $Z_2=82$ and isotopes of $N_2=126$, while the skin thickness in ^{190}Pb is approximately 0 fm.

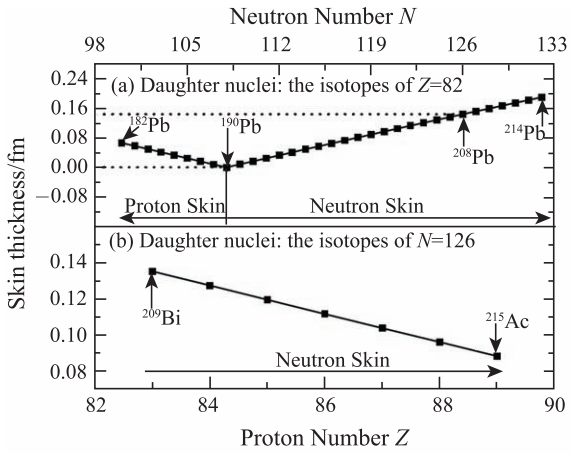

Fig. 6 The skin S with the variation of neutron number N for isotopes of $Z_2=82$ (a) and of proton number Z for isotopes of $N_2=126$ (b).

By fitting the experimental data of α-decay energy Q and half-life $T^{\rm exp}_{1/2}$ obtained from Refs. [26, 27], the parameters in Eq. (7) are obtained as $a=0.0136$, $b=-0.0165$, and $c=-14.0903$. The corresponding effect of the skin S on the α-decay half-life $T_{1/2}$ is shown in Fig. 7. It can be seen in Fig. 7(a) that the ratio for ^{190}Pb is approximately 1.0 as its skin thickness $S\approx 0$ fm. For isotopes of $Z_2=82$, the ratio ranges from 0.466 to 1.266 and the neutron skin decreases the half-life for the $^{191-214}$Pb case while the proton skin increases the half-life for the $^{182-189}$Pb case. For isotopes of $N_2=126$, the neutron skin increases the half-life with the ratio in the range of 1.279∼1.415.

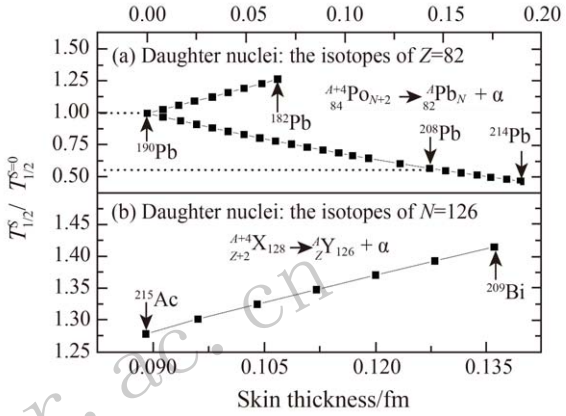

Fig. 7 The correlation between α-decay half-life ratio $T^S_{1/2}/T^{S=0}_{1/2}$ and the skin S for α decays to isotopes of $Z_2=82$ (a) and to isotopes of $N_2=126$ (b).

With above simple analysis and calculation, we find that the proton/neutron skin indeed has a considerable effect on the α-decay half-life. So the proton/neutron skin effect should be taken into account in the further studies on α-decay half lives. Actually, the skin characterizes the difference between the proton and neutron density distributions, especially in the difference in the nuclear surface region. For isotopes of $Z=82$, the difference in density distributions shall mainly affect the α-core nuclear potential. However, for isotopes of $N=126$, both the nuclear potential and the Coulomb potential will be influenced by the change of proton density distribution. More detailed information is in our other studies[15, 16].

5 Conclusion

We introduce our recent works on the clustering effects in nuclear systems. The clustering structure for ^{20}Ne and ^{9,10}Be isotopes is studied with the THSR wave function. By showing the calculated energy spectrum and the squared overlaps between THSR wave function and the RGM/GCM wave function, it is found that a single THSR wave function can provide good description for various cluster states. The non-localised aspect of cluster dynamics is discovered with the hybrid-THSR-Brink wave function, which revises

the traditional opinion that clusters occupy localized positions in the clustering states. Extensions are made for THSR wave functions to enable calculations for nuclear systems composed of both clusters and valence neutrons. It is found that these extensions are very suitable and provides good descriptions for the nuclear molecular orbit structures in low lying states of ^{9,10}Be isotopes. We also investigate the α-decay process for proton/neutron-rich nuclei. Calculated results show that the effect of proton/neutron skin is considerable on α-decay half-life.

References:

[1] TOHSAKI A, HORIUCHI H, SCHUCK P, *et al.* Phys Rev Lett, 2001, **87**: 192501.
[2] FUNAKI Y, HORIUCHI H, TOHSAKI A, *et al.* Prog. Theor Phys, 2002, **108**: 297.
[3] ZHOU B, REN Z, XU C, *et al.* Phys Rev C, 2012, **86**: 014301.
[4] ZHOU B, FUNAKI Y, HORIUCHI H,*et al.* Phys Rev Lett, 2013, **110**: 262501.
[5] ZHOU B, FUNAKI Y, HORIUCHI H, *et al.* Phys Rev C, 2014, **89**: 034319.
[6] SUHARA T, FUNAKI Y, ZHOU B, *et al.* Phys Rev Lett, 2014, **112**: 062501.
[7] LYU M, REN Z, ZHOU B, *et al.* Phys Rev C, 2015, **91**: 014313.
[8] LYU M, REN Z, ZHOU B, *et al.* Phys Rev C, 2016, **93**: 054308.
[9] YAMADA T, SCHUCK P. Eur Phys J A, 2005, **26**: 185.
[10] XU C, REN Z. Phys Rev C, 2006, **73**: 041301.
[11] REN Y, REN Z. Phys Rev C, 2012, **85**: 044608.
[12] REN Y, REN Z. Nucl Sci Tech, 2013, **24**: 050518.
[13] QIAN Y, REN Z. J Phys G-Nucl Part Phys, 2016, **43**: 065102.
[14] NI D, REN Z. Phys Rev C, 2016, **93**: 054318.
[15] NI D, REN Z. Phys Rev C, 2015, **92**: 054322.
[16] WAN N, XU C, REN, Z. Nucl Sci Tech, 2017, **28**: 22.
[17] NI D, REN Z, DONG T, XU C. Phys Rev C, 2008, **78**: 044310.
[18] KOBAYASHI F, KANADA-EN'YO Y. Prog Theor Phys, 2011, **126**: 457.
[19] KOBAYASHI F, KANADA-EN'YO Y. Phys Rev C, 2012, **86**: 064303.
[20] SUHARA T, KANADA-EN'YO Y. Prog Theor Phys, 2010, **123**: 303.
[21] KRANE K S. Introductory Nuclear Physics[M]. New York: Wiley, University of Michigan, 1987.
[22] LU X T. Nuclear Physics[M]. Beijing: Atomic Energy Press, 2008. (in Chinese)
(卢希庭. 原子核物理[M]. 北京: 原子能出版社, 2008.)
[23] GURVITZ S A, KALBERMANN G. Phys Rev Lett, 1987, **59**: 262.
[24] WALECKA J D. Theoretical Nuclear and Subnuclear Physics[M]. London: Imperial College Press, 2004.
[25] TARBERT C M. Phys Rev Lett, 2014, **112**: 242502.
[26] AUDI G, WANG M, WAPSTRA A H, *et al.* Chin Phys C, 2012, **36**: 1287.
[27] FIRESTONE R B, SHIRLEY V S, BAGLIN C M, *et al.* Table of Isotopes, 8th ed[M]. New York: Wiley Interscience, 1996.

原子核的结团效应研究

任中洲[1,2,1)]，吕梦蛟[1]，万 牛[1]

(1. 南京大学物理学院，南京 210093;
2. 兰州重离子加速器国家实验室原子核理论研究中心，兰州 730000)

摘要： 介绍了近期关于原子核结团效应的研究。利用 Tohsaki-Horiuchi-Schuck-Röpke (THSR) 波函数研究了 ^{20}Ne 和 ^{9,10}Be 等原子核的结团结构。研究发现单个的THSR波函数即可很好地描述原子核的结团态。利用 hybrid-THSR-Brink 波函数，发现了原子核结团的非局域化动力学性质。拓展了 THSR 波函数并使其能够应用于 $N \neq Z$ 的原子核之中。这一波函数正确地重现了 ^{9,10}Be 同位素的较低能级中的核分子轨道结构。还讨论了丰质子/中子原子核中的 α-衰变过程。研究发现质子/中子皮对α-衰变寿命有显著影响。

关键词： 结团结构；非局域化结团动力学；丰中子核；α-衰变

收稿日期： 2016-12-14；　**修改日期：** 2017-05-02

基金项目： 国家自然科学基金资助项目(11535004, 11035001, 11375086, 11105079, 10735010, 10975072, 11175085, 11235001)；国家重点基础研究发展计划(973计划)(2013CB834400, 2010CB327803)

1)　E-mail: zren@nju.edu.cn。